Monthly Notices
of the
ROYAL ASTRONOMICAL SOCIETY

MNRAS **444,** 3684–3698 (2014) doi:10.1093/mnras/stu1713

Dwarf galaxies in CDM and SIDM with baryons: observational probes of the nature of dark matter

Mark Vogelsberger,[1⋆] Jesus Zavala,[2†] Christine Simpson[3] and Adrian Jenkins[4]

[1]*Department of Physics, Kavli Institute for Astrophysics and Space Research, Massachusetts Institute of Technology, Cambridge, MA 02139, USA*
[2]*Dark Cosmology Centre, Niels Bohr Institute, University of Copenhagen, Juliane Maries Vej 30, DK-2100 Copenhagen, Denmark*
[3]*Heidelberg Institute for Theoretical Studies, Schloss-Wolfsbrunnenweg 35, D-69118 Heidelberg, Germany*
[4]*Institute for Computational Cosmology, Durham University, South Road, Durham DH1 3LE, UK*

Accepted 2014 August 17. Received 2014 August 5; in original form 2014 May 19

ABSTRACT

We present the first cosmological simulations of dwarf galaxies, which include dark matter self-interactions and baryons. We study two dwarf galaxies within cold dark matter, and four different elastic self-interacting scenarios with constant and velocity-dependent cross-sections, motivated by a new force in the hidden dark matter sector. Our highest resolution simulation has a baryonic mass resolution of $1.8 \times 10^2\,\mathrm{M}_\odot$ and a gravitational softening length of 34 pc at $z = 0$. In this first study we focus on the regime of mostly isolated dwarf galaxies with halo masses $\sim 10^{10}\,\mathrm{M}_\odot$ where dark matter dynamically dominates even at sub-kpc scales. We find that while the global properties of galaxies of this scale are minimally affected by allowed self-interactions, their internal structures change significantly if the cross-section is large enough within the inner sub-kpc region. In these dark-matter-dominated systems, self-scattering ties the shape of the stellar distribution to that of the dark matter distribution. In particular, we find that the stellar core radius is closely related to the dark matter core radius generated by self-interactions. Dark matter collisions lead to dwarf galaxies with larger stellar cores and smaller stellar central densities compared to the cold dark matter case. The central metallicity within 1 kpc is also larger by up to ∼15 per cent in the former case. We conclude that the mass distribution and characteristics of the central stars in dwarf galaxies can potentially be used to probe the self-interacting nature of dark matter.

Key words: methods: numerical – galaxies: haloes – dark matter.

1 INTRODUCTION

Low-mass galaxies are arguably the best places to test dark matter (DM) models since they are dynamically dominated by the DM haloes they are embedded in well within their inner regions. The kinematical information that is inferred from low surface brightness galaxies (e.g. Kuzio de Naray, McGaugh & de Blok 2008), nearby field dwarf galaxies (e.g. de Blok et al. 2008; Oh et al. 2008) and Milky Way (MW) dwarf spheroidals (dSphs; e.g. Walker & Peñarrubia 2011; Amorisco, Zavala & de Boer 2014) seems to favour the presence of $\mathcal{O}(1\,\mathrm{kpc})$ dark matter cores with different degrees of certainty. The former two cases are more strongly established while the latter is still controversial (e.g. Breddels & Helmi 2013), which is unfortunate since the MW dSphs have the largest dynamical mass-to-light ratios and are thus particularly relevant to test the DM nature. Although not necessarily related to the existence of cores, it has also been pointed out that the population of dark satellites obtained in cold dark matter (CDM) *N*-body simulations are too centrally dense to be consistent with the kinematics of the MW dSphs (Boylan-Kolchin, Bullock & Kaplinghat 2011, 2012). This problem possibly also extends to isolated galaxies (Ferrero et al. 2012; Kirby et al. 2014).

The increasing evidence of lower than expected central DM densities among DM-dominated systems is a lasting challenge to the prevalent collisionless CDM paradigm. On the other hand, the low stellar-to-DM content of dwarf galaxies represents a challenge for galaxy formation models since these have to explain the low efficiency of conversion of baryons into stars in dwarf galaxies. It is possible that these two outstanding issues share a common solution rooted in our incomplete knowledge of processes that are key to understand how low-mass galaxies form and evolve: gas cooling, star formation and energetic feedback from supernovae (SNe). In particular, episodic high-redshift gas outflows driven by SNe have been proposed as a mechanism to suppress subsequent star

⋆ E-mail: mvogelsb@mit.edu
† Marie Curie fellow.

formation and lower, irreversibly, the central DM densities (e.g. Navarro, Eke & Frenk 1996; Pontzen & Governato 2012). Although such mechanism seemingly produces intermediate-mass galaxies (halo mass $\sim 5-10 \times 10^{10}\,\mathrm{M}_{\odot}$) with realistic cores and stellar-to-halo mass ratios (Governato et al. 2010, 2012), it is questionable if it is energetically viable for lower mass galaxies (Peñarrubia et al. 2012; Garrison-Kimmel et al. 2013). Even though environmental effects such as tidal stripping might alleviate this stringent energetic condition in the case of satellite galaxies (Zolotov et al. 2012; Brooks et al. 2013; Arraki et al. 2014), the issue of low central DM densities seems relevant even for isolated galaxies (Ferrero et al. 2012; Kirby et al. 2014). This seems to indicate that SNe-driven outflows can only act as a solution to this problem if they occur very early, when the halo progenitors of present-day dwarfs were less massive (Teyssier et al. 2013; Amorisco et al. 2014). It remains unclear if such systems can avoid regenerating a density cusp once they merge with smaller, cuspier haloes. It is also far from a consensus that the implementation of strong 'bursty' star formation recipes in simulations, a key ingredient to reduce central DM densities, is either realistic or required to actually produce consistent stellar-to-halo mass ratios (e.g. Marinacci, Pakmor & Springel 2014a), and other observed properties. It is therefore desirable, but challenging, to identify observables that could unambiguously determine whether bursty star formation histories with a strong energy injection efficiency (into the DM particles) are realistic or not.

An exciting alternative solution to the problems of CDM at the scale of dwarfs is that of self-interacting dark matter (SIDM). Originally introduced by Spergel & Steinhardt (2000), it goes beyond the CDM model by introducing significant self-collisions between DM particles. The currently allowed limit to the self-scattering cross-section is imposed more stringently by observations of the shapes and mass distribution of elliptical galaxies and galaxy clusters (Peter et al. 2013), and is set at $\sigma/m_{\chi} < 1\,\mathrm{cm}^2\,\mathrm{g}^{-1}$. DM particles colliding with roughly this cross-section naturally produce an isothermal core with a $\mathcal{O}(1\,\mathrm{kpc})$ size in low-mass galaxies, close to what is apparently observed. SIDM is well motivated by particle physics models that introduce new force carriers in a hidden DM sector (e.g. Arkani-Hamed et al. 2009; Feng et al. 2009; Feng, Kaplinghat & Yu 2010; van den Aarssen, Bringmann & Pfrommer 2012; Cyr-Racine & Sigurdson 2013; Tulin, Yu & Zurek 2013; Cline et al. 2014), which predict velocity-dependent self-scattering cross-sections. In the case of massless bosons for instance, the cross-section scales as v^{-4} as in Rutherford scattering. The renewed interest in SIDM has triggered a new era of high-resolution DM-only SIDM simulations: velocity dependent in Vogelsberger, Zavala & Loeb (2012, hereafter VZL), and velocity independent in Rocha et al. (2013), that hint at a solution to the CDM problems in low-mass galaxies. In particular for the MW dSphs, it has been established that the resultant dark satellites of a MW-size halo are consistent with the dynamics of the MW dSphs, have cores of $\mathcal{O}(1\,\mathrm{kpc})$ and avoid cluster constraints only if $0.6\,\mathrm{cm}^2\,\mathrm{g}^{-1} \lesssim \sigma/m_{\chi} \lesssim 1.0\,\mathrm{cm}^2\,\mathrm{g}^{-1}$, or if the cross-section is velocity dependent (Zavala, Vogelsberger & Walker 2013). Recently, simulations of SIDM models with new light mediators have shown that is possible to also suppress the abundance of dwarf galaxies due to the modified early-Universe power spectrum caused by the interactions of the DM with the dark radiation (Boehm et al. 2014; Buckley et al. 2014).

Given the recent success of SIDM, a natural step is to elevate its status to that of CDM by studying the synergy between baryonic physics and DM collisionality in a suitable galaxy formation model. So far, this has been studied only analytically (Kaplinghat et al. 2014), with a focus in more massive galaxies where baryons dominate the central potential. Interestingly, in this case, the DM core size is reduced and the central densities are higher compared to SIDM simulations without the effect of baryons. In this paper we concentrate on the regime of dwarf galaxies by pioneering cosmological hydrodynamical simulations that include the physics of galaxy formation within a SIDM cosmology. We compare them with their counterparts (under the same initial conditions) in the CDM model with the main objective of understanding the impact of SIDM on the formation and evolution of dwarf galaxies.

This paper is organized as follows. We describe our simulations and the DM models that we explore in Section 2. We continue with Section 3, where we give a first visual impression of our dwarf galaxies. After that we provide more quantitative results in Section 4, where we focus on global properties of the dwarf galaxies and haloes forming in the different DM models. We study the various spherically averaged profiles of the dwarfs in Section 5. In Section 6 we focus on the inner parts of the haloes, where we expect the largest changes due to self-interactions. We summarize our results in Section 7.

2 SIMULATIONS

To be consistent with our previous work (VZL), we generate zoom-in initial conditions for two dwarf galaxies from the Millennium-II Simulation (MS-II; Boylan-Kolchin et al. 2009). The MS-II initial conditions, as the Aquarius initial conditions studied in our previous SIDM work, use the following cosmological parameters: $\Omega_{\mathrm{m}} = \Omega_{\mathrm{dm}} + \Omega_{\mathrm{b}} = 0.25$, $\Omega_{\mathrm{b}} = 0.04$, $\Omega_{\Lambda} = 0.75$, $h = 0.73$, $\sigma_8 = 0.9$ and $n_{\mathrm{s}} = 1$; where Ω_{m} (with contributions from DM, Ω_{dm}, and baryons, Ω_{b}) and Ω_{Λ} are the contributions from matter and cosmological constant to the mass/energy density of the Universe, respectively, h is the dimensionless Hubble constant parameter at redshift zero, n_{s} is the spectral index of the primordial power spectrum and σ_8 is the rms amplitude of linear mass fluctuations in $8\,h^{-1}$ Mpc spheres at redshift zero.

Our simulations include baryons and related astrophysical processes. We employ the implementation of Vogelsberger et al. (2013) for the moving mesh code AREPO (Springel 2010). We stress that we do not change any parameters of the model, i.e. we use the same physics parametrization as the large-scale simulations in Vogelsberger et al. (2013) and Torrey et al. (2014) and the zoom-in MW simulations of Marinacci et al. (2014a,b) and Pakmor, Marinacci & Springel (2014) (with minor modifications). Recently, this model was also employed to run the Illustris simulation (see Genel et al. 2014; Vogelsberger et al. 2014a,b, for more details). The model includes: gas cooling and photoionization, star formation and physics of the interstellar medium, stellar evolution, gas recycling, chemical enrichment and kinetic stellar SN feedback. We note that we do not include supermassive black holes and active galactic nuclei (AGN) feedback in our simulations since this is not expected to play any role at the mass scale under consideration.

The implementation for elastic DM self-scattering follows VZL, where DM interactions are modelled with a Monte Carlo approach. We have ported this implementation from GADGET to AREPO without major changes, and we consider four different elastic SIDM models in this work: SIDM1, SIDM10, vdSIDMa and vdSIDMb. The first two have a constant cross-section while the last two have velocity-dependent cross-sections. The characteristics of the models are summarized in Table 1. These models were also considered in Vogelsberger & Zavala (2013) and Zavala et al. (2013) to predict direct detection signals of SIDM and to constrain the different models using data from the MW dSphs.

Table 1. DM models considered in this paper. CDM is the standard collisionless model without any self-interaction. SIDM10 is a reference model with a constant cross-section an order of magnitude larger than allowed by current observational constraints. We note that such a model could still be realized in nature if this large cross-section would only hold over a limited relative velocity range. SIDM1 is also a model with constant cross-section, which is potentially in the allowed range. vdSIDMa and vdSIDMb have a velocity-dependent cross-section motivated by the particle physics model presented in Feng et al. (2009) and Loeb & Weiner (2011). These two models are allowed by all astrophysical constraints, and solve the 'too big to fail' problem (see Boylan-Kolchin et al. 2011) as demonstrated in VZL.

Name	$\sigma_{\rm T}^{\rm max}/m_\chi$ (cm^2 g^{-1})	$v_{\rm max}$ (km s^{-1})	Allowed?
CDM	–	–	Yes
SIDM1	1	–	Maybe
SIDM10	10	–	No
vdSIDMa	3.5	30	Yes
vdSIDMb	35	10	Yes

Table 2. Summary of the simulations. The two dwarf galaxies (dA, dB) are simulated in CDM and four different SIDM models (SIDM1, SIDM10, vdSIDMa, vdSIDMb) with (B) and without baryons. We list the DM particle mass resolution ($m_{\rm dm}$), the cell target mass ($m_{\rm baryon}$), the Plummer-equivalent maximum physical softening length (ϵ) and the number of DM particles in the high-resolution region. The simulations contain initially the same number of gas cells in the high-resolution region. All models for each halo are simulated with the same numerical resolution, except for dA-CDM, which was simulated with an eight times higher mass resolution (dA-CDM-B-hi) to check for convergence.

Name	$m_{\rm dm}$ (10^2 M$_\odot$)	$m_{\rm baryon}$ (10^2 M$_\odot$)	ϵ (pc)	$N_{\rm DM}^{\rm hires}$
dA-CDM-B-hi	9.7	1.8	34.2	122 729 602
dA-CDM-B	77.5	14.8	68.5	15353 772
dA-SIDM1-B	77.5	14.8	68.5	15353 772
dA-SIDM10-B	77.5	14.8	68.5	15353 772
dA-vdSIDMa-B	77.5	14.8	68.5	15353 772
dA-vdSIDMb-B	77.5	14.8	68.5	15353 772
dA-CDM	77.5	–	68.5	15353 772
dA-SIDM1	77.5	–	68.5	15353 772
dA-SIDM10	77.5	–	68.5	15353 772
dA-vdSIDMa	77.5	–	68.5	15353 772
dA-vdSIDMb	77.5	–	68.5	15353 772
dB-CDM-B	406.2	77.4	82.2	8196 410
dB-SIDM1-B	406.2	77.4	82.2	8196 410
dB-SIDM10-B	406.2	77.4	82.2	8196 410
dB-vdSIDMa-B	406.2	77.4	82.2	8196 410
dB-vdSIDMb-B	406.2	77.4	82.2	8196 410
dB-CDM	406.2	–	82.2	8196 410
dB-SIDM1	406.2	–	82.2	8196 410
dB-SIDM10	406.2	–	82.2	8196 410
dB-vdSIDMa	406.2	–	82.2	8196 410
dB-vdSIDMb	406.2	–	82.2	8196 410

The resolution properties of the simulations are summarized in Table 2. We simulate two dwarf-scale haloes: dA and dB. All simulations are carried out with DM-only and with full baryonic physics (B). The softening length is initially fixed in comoving coordinates, and later (after $z = 7$) limited to a fixed length in physical coordinates, which we list in Table 2 (Plummer-equivalent softening length). We have performed one higher resolution simulation of dA for the CDM case (dA-CDM-B-hi). In this first study we will only use this simulation to demonstrate convergence of our galaxy formation model. The main analysis will be based on our default resolution. A forthcoming study will exploit dA-CDM-B-hi and higher resolution SIDM simulations to study the inner profiles in more detail (Zavala & Vogelsberger, in preparation).

We will show below that the two zoom-in regions are rather different: the dA environment hosts only one isolated dwarf galaxy, whereas the dB environment hosts two nearly equal mass isolated dwarf galaxies, which are interacting and embedded in a rich filament, i.e. the two haloes dA and dB are sampling two extreme scenarios: a very isolated dwarf with a quiescent formation history, and an interacting dwarf, which underwent several mergers in the past embedded in a strong tidal field. Some basic characteristics of the two main isolated haloes and their galaxies are listed in Table 3. Here we list virial mass ($M_{200.\rm crit}$), virial radius ($r_{200,\,\rm crit}$), maximum circular velocity ($V_{\rm max}$), DM mass ($M_{\rm DM}$), stellar mass ($M_\star$), gas mass ($M_{\rm gas}$), V-band magnitude (M_V), $B - V$ colour and baryon fraction ($f_{\rm b} = (M_\star + M_{\rm gas})/M_{200.\rm crit}$). The two haloes differ in virial mass by about a factor of 6, and by a factor of about 12 in stellar mass, which also leads to significantly different V-band magnitudes. The colours ($B - V$) of the two dwarfs are rather similar. We also include the results for the higher resolution simulation dA-CDM-B-hi to demonstrate that we achieve excellent convergence in all properties of the galaxy. We stress that this is a distinct feature of our galaxy formation model, which was built to lead to convergent results.

Is already clear from Table 3 that most of the global quantities of the galactic systems are affected only very little by the DM nature, and some relative changes are not even systematic with the amplitude of the scattering cross-section due to the stochastic character of star formation and feedback in our model. The largest systematic differences can be seen between the CDM case and the extreme SIDM10 model, but even for these two cases the relative differences are rather small. We will quantify this in more detail below.

3 VISUAL IMPRESSION

We first give some visual impressions of the simulated region at $z = 0$ in Fig. 1 (left dA, right dB): from left to right we show the projected DM density, the gas temperature and the gas metallicity. We focus here only on the most extreme models in terms of self-scattering cross-section, CDM (top) and SIDM10 (bottom). It is clear that the environments of dA and dB are very different: the dA halo is very isolated, whereas dB lives in a rich filamentary structure with other haloes surrounding it. The impact of SIDM on these scales is minimal: even the extreme SIDM10 model with a cross-section 10 times larger than observationally allowed does not alter any of the fields in a visible way on large scales. Perhaps the most visible effect in the DM distribution is a slight decrease in the abundance of (sub)haloes. We will not quantify this here in detail, but we note that a similar effect was already found in VZL for the subhalo abundance of MW-like DM haloes. However, this effect is only visible for very large cross-sections, which are observationally excluded, and is negligible for allowed models. More interesting is the fact that the modified gravitational potential of the inner region of the dwarf through its evolution leads to a different distribution of SN-driven gas outflows (clearer at smaller scales, see Fig. 2). This effect is visible in the metallicity projections, where some slight differences are noticeable even on the large scales shown

Table 3. Basic properties of the simulated dwarf galaxies dA and dB. The different columns list: virial mass ($M_{200,\,\mathrm{crit}}$), virial radius ($r_{200,\,\mathrm{crit}}$), maximum circular velocity (V_{max}), DM mass (M_{DM}), stellar mass ($M_\star$), gas mass (M_{gas}), V-band magnitude (M_V), $B-V$ colour and baryon fraction ($f_{\mathrm{b}} = (M_\star + M_{\mathrm{gas}})/M_{200,\mathrm{crit}}$). dB is about six times more massive than dA. Differences in the DM model do not lead to any significant changes in the global galaxy properties listed here. The dA-CDM-B-hi results demonstrate that our galaxy formation model leads to excellent convergence of the baryonic characteristics.

Halo name	$M_{200,\,\mathrm{crit}}$ ($10^{10}\,\mathrm{M}_\odot$)	$r_{200,\,\mathrm{crit}}$ (kpc)	V_{max} ($\mathrm{km\,s^{-1}}$)	M_{DM} ($10^8\,\mathrm{M}_\odot$)	$M_\star$ ($10^8\,\mathrm{M}_\odot$)	M_{gas} ($10^8\,\mathrm{M}_\odot$)	M_V	$B-V$	f_{b}
dA-CDM-B-hi	1.193	45.841	49.614	107.148	1.478	12.449	−15.862	0.394	0.117
dA-CDM-B	1.198	45.906	50.623	108.773	1.512	13.255	−15.941	0.382	0.123
dA-SIDM1-B	1.193	45.837	51.760	108.631	1.447	12.982	−15.947	0.371	0.121
dA-SIDM10-B	1.164	45.469	53.625	105.578	1.522	13.295	−15.963	0.386	0.127
dA-vdSIDMa-B	1.202	45.954	51.982	109.265	1.596	13.147	−16.006	0.375	0.123
dA-vdSIDMb-B	1.208	46.030	50.809	108.711	1.502	13.269	−15.935	0.389	0.122
dB-CDM-B	7.141	83.223	83.339	605.816	17.712	118.321	−18.804	0.380	0.190
dB-SIDM1-B	7.107	83.097	86.128	603.852	19.142	115.271	−18.927	0.352	0.189
dB-SIDM10-B	6.975	82.577	87.859	594.917	18.131	114.493	−18.793	0.345	0.190
dB-vdSIDMa-B	7.136	83.206	86.251	604.041	17.977	115.789	−18.738	0.372	0.187
dB-vdSIDMb-B	7.192	83.425	83.092	608.296	17.559	117.623	−18.731	0.390	0.188

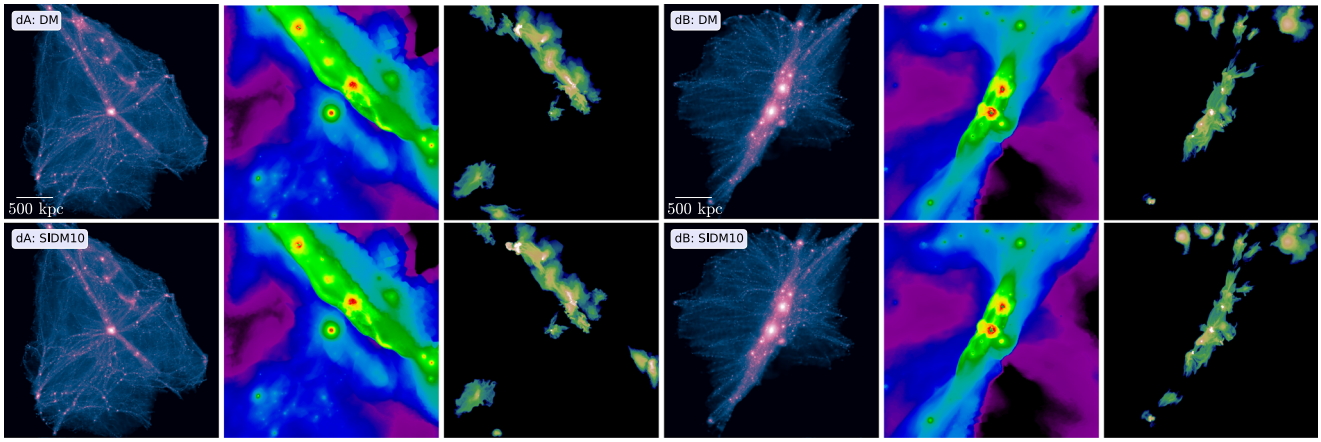

Figure 1. Visual overview of the large-scale structure around haloes dA and dB at $z = 0$ for CDM and SIDM with $\sigma/m_\chi = 10\,\mathrm{cm^2\,g^{-1}}$. We show from left to right: DM density, gas temperature and metallicity (slice thickness 500 kpc). The dA dwarf is isolated, whereas dB is embedded into a rich filament with a few other dwarfs nearby. On large scales, SIDM does not lead to any significant changes in the DM or gas distribution. The metal distribution is slightly different indicating that SN-driven outflows operate slightly differently for CDM than for SIDM due to the modified gravitational potential in the centre. However, this effect is small and stochastic in nature. The temperature structure shows no visible differences on these scales.

here. However, the effect on such large scales is very small, and it is therefore unlikely that the distribution of baryons on these scales can be used to probe the DM nature.

The build-up of the dA dwarf can be inspected in Fig. 2, where we show the evolution at five redshifts ($z = 4, 2, 1, 0.5, 0$). Here we focus only on the evolution of the gas properties: gas temperature and gas metallicity. Furthermore, we show a much smaller region around the halo compared to Fig. 1 (as indicated by the scale). It is clear that halo dA has essentially grown in isolation since $z = 4$, while halo dB has had a violent merger history (not explicitly shown here). Notice that by $z = 4$ there are only very minor differences between CDM (top panels) and SIDM10 (bottom panels), most visible in the metallicity distribution. This is because DM collisions are only relevant at lower redshifts once the densities in the centres of haloes are high enough for scatterings to occur.

The further evolution demonstrates that small variations in the inner halo DM potential due to DM collisions can alter the subsequent evolution of the galaxy. This is more spectacularly seen in the divergent history of outflows driven by SNe, which are clearly visible in the metallicity maps. However, this should be interpreted with care due to the stochastic nature of star formation and wind generation in our implementation. It seems that this is the main driver, e.g., by looking at the SFR there is no clear correlation with the amplitude of the cross-section (see Fig. 3). The conclusion seems to be that globally, this stochastic nature makes it impossible to distinguish the different DM models, which is why one needs to focus on the inner regions of the dwarfs to look for clues of DM collisions. We demonstrate below that baryonic characteristics of the inner galaxies (within ∼1 kpc) are closely related to the DM model. This is, of course, not surprising since the largest effect of SIDM occurs in the centre of galaxies through core formation.

4 GLOBAL PROPERTIES: COMPARISON TO OBSERVATIONS

We now describe the global properties, integrated over the whole galaxy, of our simulated dwarfs and compare some of them with observations of dwarf galaxies. Our intention in this work is not a detailed observational comparison, but rather to study the impact of SIDM on the baryonic component. Nevertheless, we would like

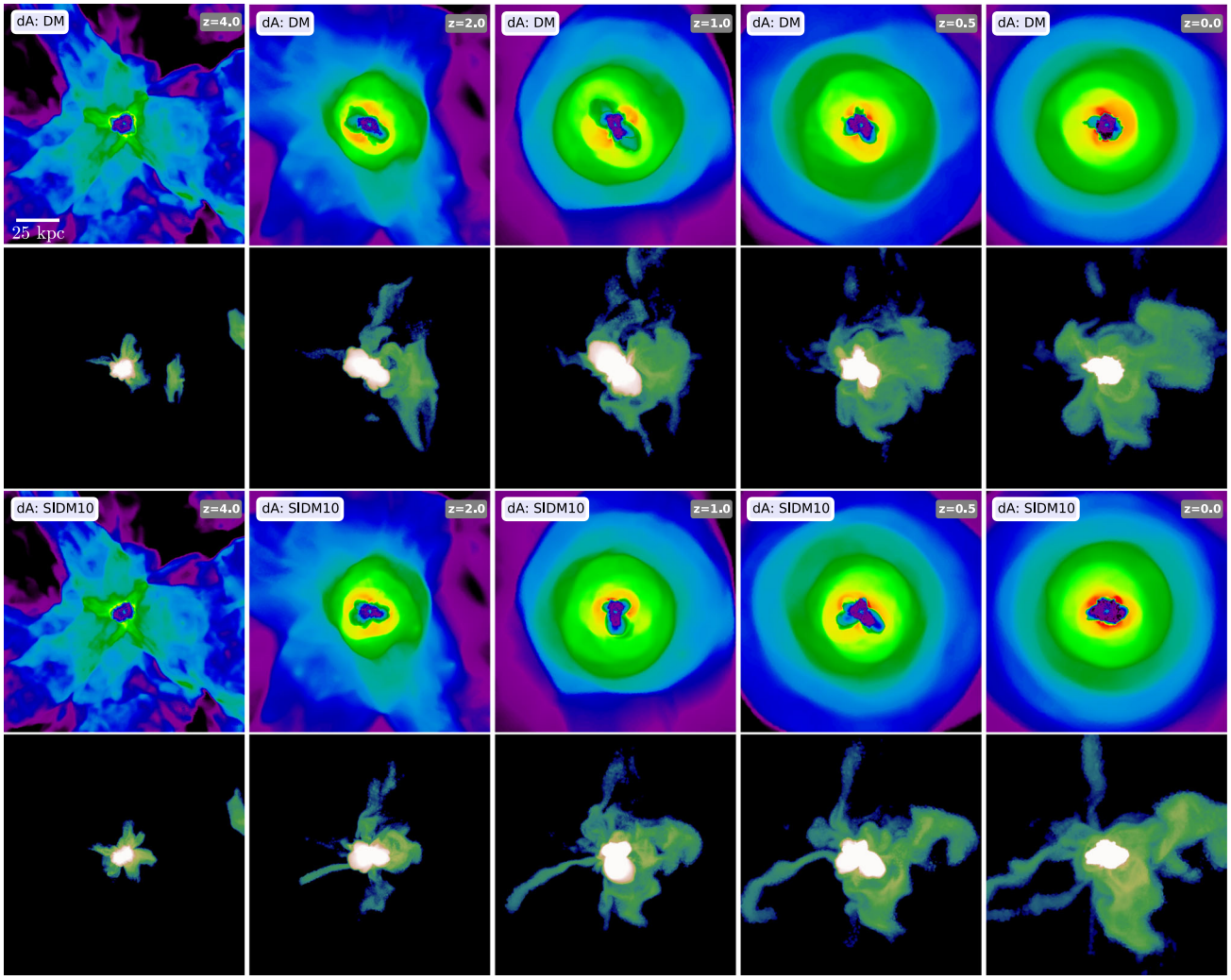

Figure 2. Redshift evolution of gas properties of dwarf dA at $z = 4, 2, 1, 0.5, 0$ (left to right). We show gas temperature (top), and gas metallicity (bottom) in slices of thickness 25 kpc. At $z = 4$, the temperature and metallicity distributions look similar in CDM and SIDM, because SIDM collisions modify the DM potential only towards later times. This then also induces changes in the baryonic evolution. The outflows seen in the metallicity maps clearly deviate between CDM and SIDM. Also the inner temperature structure is affected by this.

to quantify how 'realistic' our dwarf galaxies are in terms of their baryonic content. The comparison here is rather limited since our dwarf sample is very small, and because the model we are using is actually 'tuned' for a slightly different cosmology, and for a somewhat larger mass scale (see Vogelsberger et al. 2013, for details). With these caveats in mind, we compare the two dwarfs to a few observations below. This section will also demonstrate that the impact of SIDM on global and integrated galaxy properties is typically negligible at the mass scales we explore here.

We first study the star formation efficiency by measuring the total stellar mass within $r < r_\star$ at $z = 0$, where $r_\star$ is twice the stellar half-mass radius, which we define as our fiducial galaxy radius (see Vogelsberger et al. 2013, for details). The result is shown in the upper left-hand panel of Fig. 3 for the different scenarios according to the legend for the less massive halo (dA) and the more massive halo (dB).

We compare our results to the empirical $M_\star$–M_h relation obtained using the abundance matching technique for observed galaxies at $z = 0$ (Behroozi et al. 2013; Moster et al. 2013). Compared to these, halo dA has formed too many stars while halo dB has the right stellar mass content at $z = 0$ being within the observational 1σ uncertainties. We also include recent simulation results from Hopkins et al. (2013) and Sawala et al. (2014) (simulated in a Local Group environment), along with observational data of Local Group dwarfs (MW+M31 dSphs+dIrrs) (taken from Côté, Carignan & Freeman 2000; McGaugh 2005; Peñarrubia, McConnachie & Navarro 2008; Woo, Courteau & Dekel 2008; Stark, McGaugh & Swaters 2009; Misgeld & Hilker 2011; Oh et al. 2011; Ferrero et al. 2012; Tollerud et al. 2012). Considering all this simulation and observational data, it seems that the stellar mass of dA, albeit in the high end, is not unreasonable. Nevertheless, we still need a larger simulation sample of galaxies in that mass range to test how reasonable is the galaxy formation model we have used. Since this is not the main focus of the current paper, we leave it for future studies, concentrating instead on the contrast between the different DM models in the following sections.

In the left-hand panels in the second and third rows of Fig. 3, we show the star formation rates as a function of lookback time in 0.5 Gyr bins. For this, we consider all stellar particles which belong to the galaxy ($r < r_\star$) at $z = 0$. With this age resolution, our model

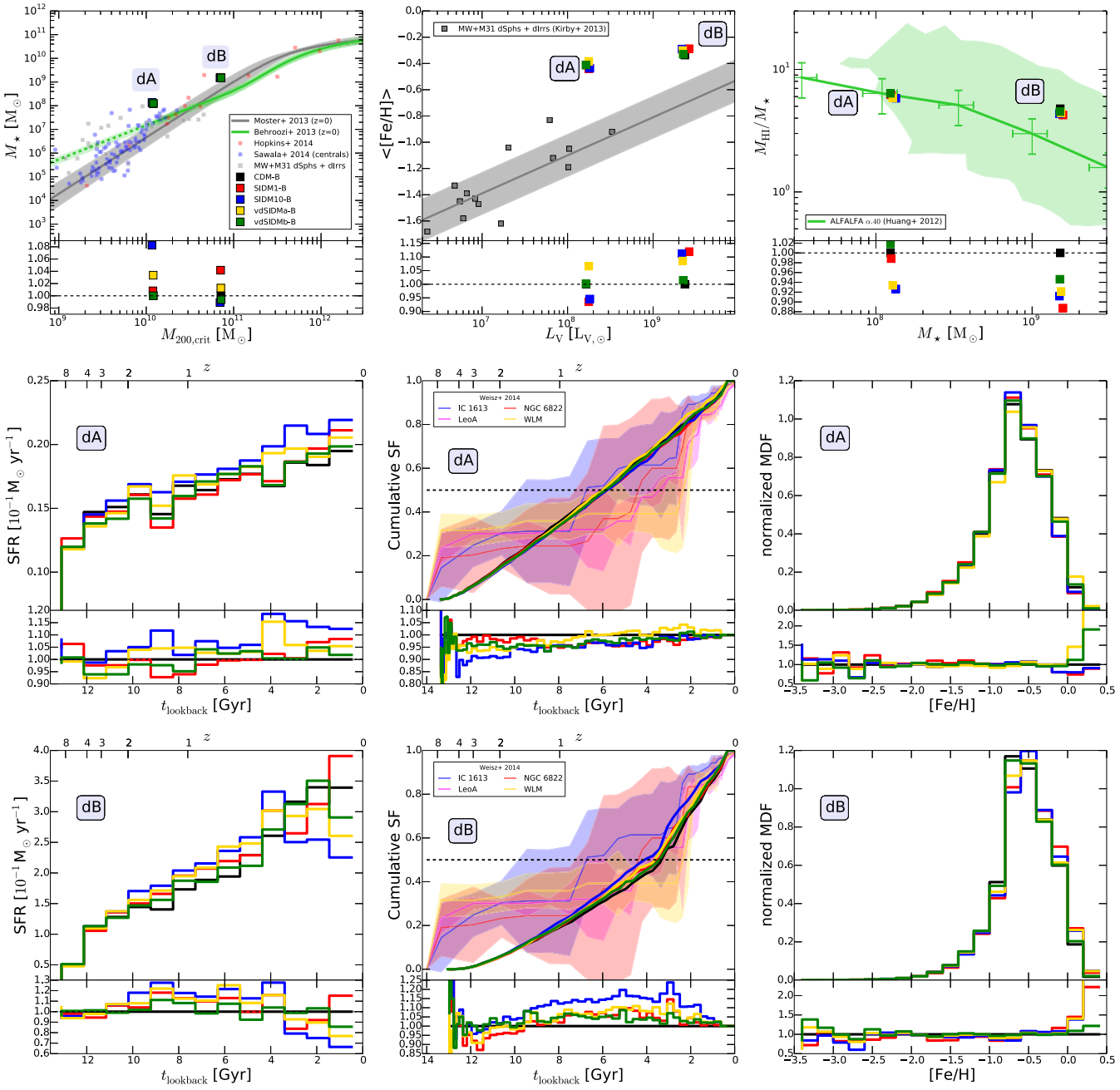

Figure 3. A selection of global properties of the simulated galaxies at $z = 0$. Top three panels (left to right): the stellar mass as a function of halo mass compared to recent abundance matching results from Moster, Naab & White (2013) and Behroozi, Wechsler & Conroy (2013), to simulation results from Hopkins et al. (2013) and Sawala et al. (2014) and to observations of Local Group dwarfs; the metallicity–luminosity relation compared to observations from Kirby et al. (2013) and the H I mass–richness relation compared to observations from Huang et al. (2012). The other six panels show for the two haloes (top: dA; bottom: dB): the star formation history in bins of 0.5 Gyr (left), the cumulative star formation history (middle) compared to four Local Group dwarfs taken from Weisz et al. (2014), which have similar stellar masses and are reasonably isolated based on the host distance, and the stellar metallicity distribution function (right). In the bottom of each panel we show the ratio of each model to that of CDM. The nature of DM (CDM versus SIDM) does not lead to any significant and systematic differences in the global properties of galaxies. Typical changes are of the order of 10 per cent at most.

does not lead to a very bursty star formation history, although the time evolution is also not completely smooth. We stress that there is currently no undisputed direct observational evidence for bursty star formation histories for dwarfs like the ones simulated here. It remains to be seen which distribution of star formation histories is actually realized in Nature. Nevertheless, we should note that a recent analysis by Kauffmann (2014) seems to give convincing evidence that most $M_\star \sim 10^8\,\mathrm{M}_\odot$ galaxies suffer ongoing bursts of star formation with a typical duration (Δt_burst) of the order of the characteristic dynamical time of the galaxy (Δt_dyn). Although this might suggest that the gas outflows from these bursts could change the DM distribution, it is not clear how efficient this would be since the highly efficient regime occurs only once $\Delta t_\mathrm{burst} \ll \Delta t_\mathrm{dyn}$.

The star formation rates of the two dwarfs show a slightly different behaviour: the rate of dA is fluctuating around a moderately non-evolving mean, whereas dB has a more significantly increasing

mean. Most importantly, none of our dwarfs has an exponentially declining star formation history. These trends are actually similar to models with more explicit stellar feedback (see Hopkins et al. 2013, for example). The middle panels in the second and third rows in Fig. 3 show the fractional cumulative star formation, i.e. the fraction of stellar mass formed before the indicated time. We compare the simulation results to a few dwarf galaxies based on a sample from Weisz et al. (2014) of four Local Group dwarf irregulars lying in a similar stellar mass range as the simulated ones and that are not disturbed too much by the tidal field of the MW and Andromeda (see e.g. fig. 1 of Leaman et al. 2012 for a visual impression). The cumulative star formation histories of our dwarf galaxies do not deviate strongly from the observational data. Notice how the observed dwarfs seem to have larger star formation rates at very early ($z > 4$) and very late times ($t_{\rm lookback} \lesssim 4\,{\rm Gyr}$) compared to our isolated dwarf (dA). The seemingly good agreement with our systems dB in the late time regime might indicate that interactions are responsible for the late time surge of star formation. However, this is only speculative since the observed dwarfs are in relative isolation today. The high-redshift regime might be related to a period of star formation before reionization and thus, to a scenario where the observed dwarfs come from progenitors that collapsed earlier than the haloes we simulate here.

In the bottom of each panel of Fig. 3, we show the ratios of the different DM models with respect to the CDM prediction. The total stellar masses have variations of the order of only ∼10 per cent and, as the star formation histories suggest, these are likely related to the stochastic nature of star formation (and SNe-driven winds) in our simulations. Looking at the star formation rates for instance, it is clear that there is no trend with the amplitude of the scattering cross-section (noticeable with more clarity by comparing the red, SIDM1, and blue, SIDM10, lines in both panels). Nevertheless, the total amount of stars tends to either be very identical to the stellar mass formed in CDM, or a few per cent higher according to the upper left-hand panel.

The upper right-hand panel of Fig. 3 shows the neutral hydrogen H I richness relation for our two galaxies compared to data from the Arecibo Legacy Fast ALFA (ALFALFA) survey (40 per cent of the catalogue of Huang et al. 2012). Both simulated galaxies lie within the observed distribution, although halo dB is more H I rich than the observed mean. The second panel in the top row shows the *V*-band luminosity–metallicity relation, where a comparison with the compilation of data for dSphs and dIrrs presented in Kirby et al. (2013) is also shown. These two types of galaxies seem to obey the same relation. Our simulated galaxies are slightly too metal rich compared to observations, particularly for the smallest dwarf. Finally, the right-hand panels in the second and third rows of Fig. 3 show the metallicity distribution functions.

The bottom panels in Fig. 3 show the relative differences between the CDM case and the SIDM models. Most of these changes are small, of the order of ∼10 per cent, and not correlated with the specific DM model, i.e. there is no clear correlation with the cross-section. Nevertheless, there are some interesting points. For instance, the total stellar mass seems to increase in most of the SIDM models. The neutral hydrogen content on the other hand is decreasing for most SIDM models compared to the CDM case. However, for both observables the effect is at maximum around 10 per cent. The changes in the star formation rate as a function of lookback time can be larger. Relative differences in each time bin can be as large as ∼20–30 per cent. As for the stellar mass, the largest differences occur for the SIDM10 model compared to the CDM case. The high-metallicity tail of the stellar MDF is also sensitive to the DM model. However, this region of the MDF is not probed very well due to low number statistics. The same is true for the low-metallicity tail of the distribution.

We conclude that all models are in reasonable agreement within the observational range although there might be potential discrepancies if the simulated galaxies represent the median of the distribution of a larger complete sample. We also conclude that allowed changes on the DM self-scattering cross-sections do not strongly affect the global properties of the two dwarfs. Most changes are of the order of 10 per cent at maximum, and we do not find any systematic trends with the specific DM model, i.e. these changes are largely stochastic and not directly correlated with the magnitude and type of SIDM cross-section.

5 THE RELEVANCE OF DM SELF-INTERACTIONS

It is expected that the impact of DM collisions will be most evident in the central regions of the dwarfs where the average number of collisions per particle across the entire history of the galaxy is larger than one. We will therefore focus on this region from here on and only refer to our isolated system dA. In Fig. 4 we show various radial profiles at $z = 0$. We show the DM density, velocity dispersion and velocity anisotropy profiles in the first row while the second row shows the same quantities for the stellar component. For the gas in the last row, we show the density and temperature profiles only. The lower right-hand panel of Fig. 4 compares the DM density profiles of the CDM and SIDM10 model for a simulation with DM particles only (CDM, SIDM10) to the full baryonic physics simulations (CDM-B, SIDM10-B). At the bottom of each panel we show the relative differences with respect to the CDM case.

The upper DM panels demonstrate that DM collisions generate an isothermal density core with a flat velocity dispersion and a spatial extent that is related to the magnitude of the scattering cross-section at the typical DM velocities of the central regions. All the allowed SIDM models have core sizes $\lesssim$2 kpc at the scale of dwarfs. We also notice that while models with a constant cross-section predict a strong dependence of the core size with halo mass (Rocha et al. 2013), the Yukawa-like vdSIDM models we explore here naturally create a much milder correlation. The behaviour of the velocity anisotropy illustrates how DM collisions isotropize the orbits of the DM particles with an amplitude that is correlated with the magnitude of the cross-section: a larger cross-section leads to a lower anisotropy.

One can clearly see that the central DM density is reduced by at least a factor of 2 at the softening scale for all SIDM models. For the most extreme model, SIDM10, the redistribution of DM particles also leads to a significant increase (∼40 per cent) of the DM density at about ∼6 per cent of $r_{200,\,\rm crit}$. This effect can also be seen for the allowed SIDM1 model although the excess is much smaller in that case (∼10 per cent), and occurs at a slightly smaller radius (∼4 per cent of $r_{200,\,\rm crit}$). The effects on the DM distribution are always largest in the SIDM10 case. This is also true for the anisotropy parameter $\beta_{\rm DM}$ which is essentially zero within 10 per cent of $r_{200,\,\rm crit}$ for the SIDM10 model. The transition to this isotropic velocity distribution is much smoother for the other SIDM models, but all of them reach $\beta_{\rm DM} \sim 0$ in the inner part of the halo, whereas the CDM goes down to slightly larger values only ($\beta_{\rm DM} \sim 0.1$). Self-interactions play a role only in the inner part ($\lesssim$ 1 kpc) of the halo such that the outer profiles agree well between the different models. However, the most extreme model, SIDM10,

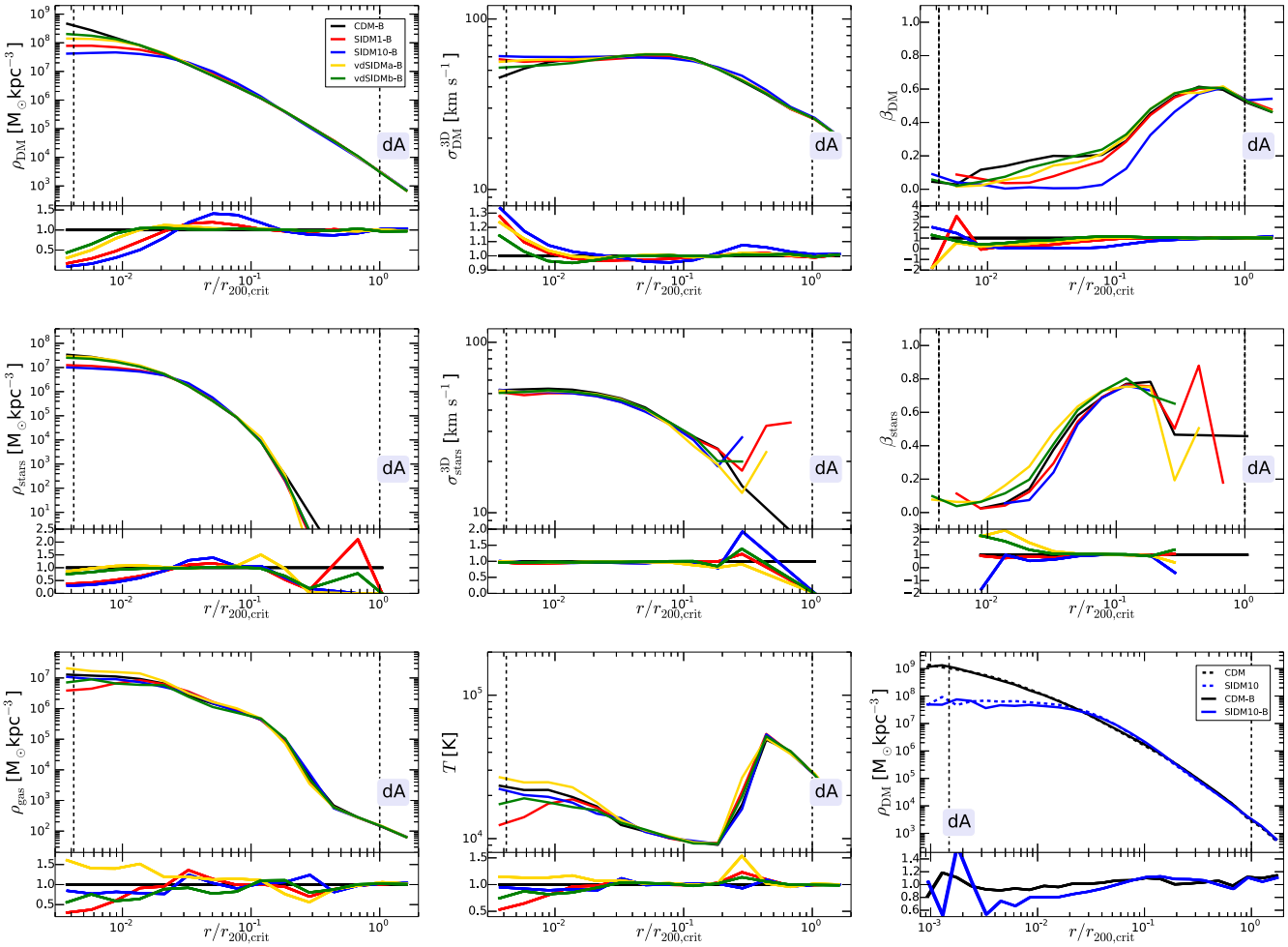

Figure 4. Radial profiles for halo dA. We show from top left to bottom right: DM density, DM velocity dispersion, DM velocity anisotropy, stellar density, stellar velocity dispersion, stellar velocity anisotropy, gas density, gas temperature, and in the last panel the DM density profile for the CDM and SIDM10 models with and without baryons. Most profiles of halo dB look similar with respect to the difference between the different DM models. However, the dB halo is less relaxed due to its environment. This affects, for example, the anisotropy (β) profile, which for dB is not monotonically decreasing towards the halo centre. The dotted vertical lines mark 2.8 times the softening length and the mean virial radius.

shows significant deviations in the density and velocity structure even out to ∼30 per cent of $r_{200,\,\rm crit}$.

The stellar distribution is also clearly affected by self-interactions. The relative differences between CDM and SIDM are largest for the inner density and anisotropy profiles. The SIDM10 and SIDM1 models lead to a decrease in the central stellar density of more than a factor of 2. Although the SIDM10 model is ruled out due to its large cross-section, SIDM1 is still a possible CDM alternative, which leads to a significant modification of the central stellar density. Similar to the DM density, the SIDM1 and SIDM10 stellar densities also exceed the stellar density of the CDM model around 5 per cent of $r_{200,\,\rm crit}$. Interestingly, the velocity dispersion profile $\sigma^{\rm 3D}_{\rm stars}$ is not altered significantly through self-interactions. Also the velocity anisotropy profiles of the stars are more similar, between the different simulations, than those of DM.

The gas density profile in the lowest row of the figure also shows deviations of about a factor of 2. Except for vdSIDMa, all models behave similar to the findings of the DM and stellar profiles, i.e. a significant reduction of the gas density in the centre. vdSIDMa, on the other hand, shows an increased gas density at the centre. Also, the central temperature of vdSIDMa is higher than all other models. For SIDM1, the temperature is only 50 per cent of the gas temperature in the CDM gas. However, it seems that the changes in the gas are less correlated with the actual cross-section than those in the DM and stellar component. For example, the largest differences in the gas density and temperature can be seen for SIDM1 and not for the more extreme model SIDM10. Also vdSIDMa shows the opposite behaviour compared to the other SIDM models.

The lower right-hand panel of Fig. 4 demonstrates that the feedback associated with SNe does not alter the DM density distribution in our model. This is not surprising since we do not employ a very bursty star formation model, but a rather smooth star formation prescription. As a consequence, the DM density profile is not affected at all by the formation of the baryonic galaxy and the related feedback processes for the CDM case. The SIDM models lead to core formation due to self-interactions of DM particles. Such core makes it easier for SNe feedback to drive gas outwards, which should cause some effect on the DM distribution. In fact, the lower right-hand panel of Fig. 4 demonstrates that the DM density is slightly reduced in the cored region even with a smooth feedback model like ours. However, this effect is rather small and at maximum ∼40 per cent relative to the SIDM10 simulation without baryons. This effect is therefore small compared to the effect of self-interactions, which reduce the central DM density much more significantly.

Table 4. Best-fitting parameters to the DM, stellar and gas density and anisotropy profiles. The different columns list: the name of the DM model and the component under consideration, the profile that was fit to that component and the parameters of the profiles obtained for the best fit. In the case of the double component fits for the stars and for the gas, the goodness of the fit (equation 6) is computed for the combined fit. In the case of stars, the fit is restricted to the region within 10 kpc. On the left we list the best-fitting parameters for the density profiles and on the right those for the velocity anisotropy profiles. For the latter, we do not distinguish inner and outer regions for the stars, and we do not give a profile for the gas. We stress that we provide different DM density profiles for the different DM models since a single parametric model cannot be used to achieve a good fit to all models.

Component	ρ profile	ρ ($M_\odot$ kpc^{-3})	r_s (kpc)	r_c (kpc)	α	β profile	A	a	α_β	b	β_0
CDM-B											
Dark matter	NFW equation (1)	4.41×10^7	1.97	–	–	Equation (8)	0.083	1.265	0.385	0.541	0.071
Stars (inner)	Cored/exp. equation (5)	5.24×10^6	–	0.46	2.44	Equation (8)	42.29	2.790	5.082	0.312	−0.060
Stars (outer)	Cored/exp. equation (5)	1.05×10^7	0.80	–	–	Equation (8)	42.29	2.790	5.082	0.312	−0.060
Gas (inner)	Cored/exp. equation (5)	1.16×10^7	–	0.98	3.00	Equation (8)	–	–	–	–	–
Gas (outer)	Cored/exp. equation (5)	6.98×10^6	1.88	–	–	Equation (8)	–	–	–	–	–
SIDM1-B											
Dark matter	Burkert like equation (3)	3.34×10^8	1.00	3.74	–	Equation (8)	2.011	2.382	3.807	0.262	0.000
Stars (inner)	Cored/exp. equation (5)	6.44×10^6	–	0.77	2.49	Equation (8)	21.62	3.222	4.766	0.358	−0.017
Stars (outer)	Cored/exp. equation (5)	1.29×10^7	0.75	–	–	Equation (8)	21.62	3.222	4.766	0.358	−0.017
Gas[a]	Cored/exp. equation (5)	7.43×10^6	1.80	–	–	Equation (8)	–	–	–	–	–
SIDM10-B											
Dark matter	Equation (2)	1.48×10^8	–	1.55	2.82	Equation (8)	0.727	3.258	4.358	0.278	0.000
Stars (inner)	Cored/exp. equation (5)	7.62×10^6	–	0.90	2.37	Equation (8)	25.54	3.475	4.986	0.368	−0.049
Stars (outer)	Cored/exp. equation (5)	1.40×10^7	0.74	–	–	Equation (8)	25.54	3.475	4.986	0.368	−0.049
Gas (inner)	Cored/exp. equation (5)	9.01×10^6	–	0.88	1.69	Equation (8)	–	–	–	–	–
Gas (outer)	Cored/exp. equation (5)	5.56×10^6	2.10	–	–	Equation (8)	–	–	–	–	–
vdSIDMa-B											
Dark matter	Burkert like equation (3)	1.33×10^9	0.64	5.13	–	Equation (8)	1.032	1.892	2.672	0.281	0.000
Stars (inner)	Cored/exp. equation (5)	5.82×10^6	–	0.56	2.80	Equation (8)	114.5	2.816	5.983	0.289	0.015
Stars (outer)	Cored/exp. equation (5)	1.09×10^7	0.81	–	–	Equation (8)	114.5	2.816	5.983	0.289	0.015
Gas (inner)	Cored/exp. equation (5)	1.23×10^7	–	0.87	2.91	Equation (8)	–	–	–	–	–
Gas (outer)	Cored/exp. equation (5)	9.47×10^6	1.68	–	–	Equation (8)	–	–	–	–	–
vdSIDMb-B											
Dark matter	Burkert like equation (4)	8.49×10^7	1.57	0.30	–	Equation (8)	0.142	0.983	0.286	0.553	0.000
Stars (inner)	Cored/exp. equation (5)	5.66×10^6	–	0.57	2.66	Equation (8)	37.28	3.424	5.250	0.361	0.042
Stars (outer)	Cored/exp. equation (5)	1.17×10^7	0.77	–	–	Equation (8)	37.28	3.424	5.250	0.361	0.042
Gas (inner)	Cored/exp. equation (5)	1.82×10^7	–	1.26	3.90	Equation (8)	–	–	–	–	–
Gas (outer)	Cored/exp. equation (5)	6.23×10^6	1.90	–	–	Equation (8)	–	–	–	–	–

[a]In this case the fit is poor in the inner regions ($\lesssim$ 1.5 kpc), and thus, we use only the exponential gas profile instead of the two-component model as in the other cases.

So far we have discussed the relative differences between the different profiles. To quantify the spatial distribution of the DM and the baryons, gas and stars, in more detail, we now find analytical fits to the spherically averaged density distributions. We have found that the different DM models require different density profiles to achieve a reasonable quality of the fits.

We start with the DM profile for the CDM case. It is well known that CDM haloes have spherically averaged density profiles that are well described by Navarro–Frenk–White (NFW; Navarro et al. 1996) or Einasto profiles (Springel et al. 2008). We therefore fit the DM profile of the CDM model with the two-parameter NFW profile:

$$\rho_{\rm CDM}(r) = \rho_0 \frac{r_{\rm s}^3}{r(r+r_{\rm s})^2}. \quad (1)$$

On the other hand, the SIDM haloes are well fitted by cored-like profiles that vary according to the amplitude of the self-scattering cross-section at the typical velocities of the halo. In the case of the strongest cross-section, SIDM10, a good fit is obtained with the following three-parameter profile:

$$\rho_{\rm SIDM10}(r) = \rho_0 \frac{r_{\rm c}^\alpha}{(r_{\rm c}^\alpha + r^\alpha)}, \quad (2)$$

while for intermediate cross-sections, SIDM1 and vdSIDMa, a Burkert-like three-parameter formula provides a better fit:

$$\rho_{\rm (SIDM1,vdSIDMa)}(r) = \rho_0 \frac{r_{\rm s}^3}{(r+r_{\rm c})(r^2+r_{\rm s}^2)}. \quad (3)$$

Finally, for the weakest cross-section, vdSIDMb, a good fit is given by

$$\rho_{\rm (vdSIDMb)}(r) = \rho_0 \frac{r_{\rm s}^3}{(r+r_{\rm c})(r+r_{\rm s})^2}. \quad (4)$$

Next we consider the profiles of the baryonic components. For the stars and the gas, we use a two-component density profile: an exponential profile in the outer region, which is a good approximation

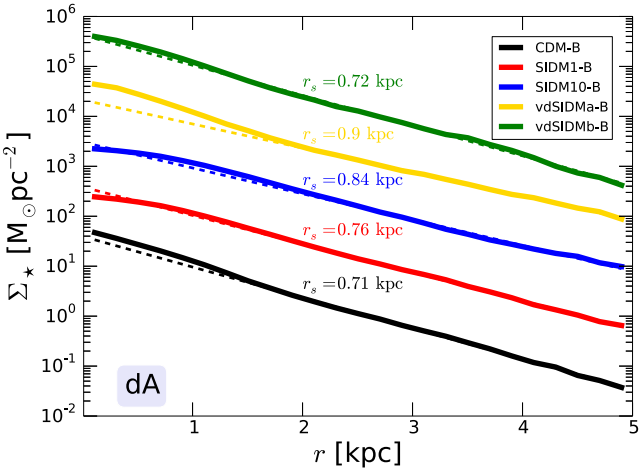

Figure 5. Stellar surface density profiles with exponential fits (dashed lines) for halo dA for all DM models. The non-CDM cases are shifted up by factors of 10. Exponential scale lengths, r_s, are stated for each fit. The fits were performed over the full radial range. All models lead to essentially perfect exponential profiles with no significant bulge components. The largest cross-section models (SIDM1, SIDM10) produce a stellar core in the centre.

except for the gas beyond ∼20 kpc, and a cored profile in the inner region, analogous to equation (2):

$$\rho_{(\star,\mathrm{gas})}(r) = \begin{cases} \rho_{\mathrm{out},(\star,\mathrm{gas})}\ \exp(-\frac{r}{r_{\mathrm{s},(\star,\mathrm{gas})}}) & r \geq r_{\mathrm{in}}, \\ \rho_{\mathrm{in},(\star,\mathrm{gas})}\ \frac{r_{\mathrm{c}}^{\alpha}}{r_{\mathrm{c}}^{\alpha}+r^{\alpha}} & r < r_{\mathrm{in}}, \end{cases} \tag{5}$$

where we find that $r_{\mathrm{in}} = 1.5$ kpc provides a good fit in all cases except for the gas distribution in the SIDM1 case.

For each profile (DM, gas and stars), we find the best-fitting parameters by minimizing the following estimate of the goodness of the fit:

$$Q^2 = \frac{1}{N_{\mathrm{bins}}} \sum_i \left(\ln\rho_i(r_i) - \ln\rho_{\mathrm{fit}}(r_i)\right)^2, \tag{6}$$

where the sum goes over all radial bins. We summarize the best-fitting parameters for each component in Table 4.

We stress again that we need distinct parametric density profiles to better describe the spatial DM structure of the halo for the different DM models. For instance, in the case of SIDM10, the value of Q for the best fit using equation (2) is 0.004, whereas using equations (3) and (4) values are 0.008 and 0.074, respectively. On the other hand, for SIDM1, the values of Q using equations (2)–(4) are, respectively, 0.020, 0.003, 0.021. Clearly, in this case, equation (3) is the best fit.

For the stars we can also inspect the stellar surface density profiles which are closely related to the measured stellar surface brightness profiles. The stellar surface density profiles of the dA dwarfs for the different DM models are shown in Fig. 5. The exponential scale length, r_s, of the different models is quoted for each model, and the dashed lines show the actual exponential fits for each model. For the CDM case, we find over a large radial range an exponential profile and no significant bulge contribution, similar to what is observed for most dwarfs. We have checked that the surface density profiles do not vary much if the orientation of the galaxy changes. The reason for this is that the dwarfs do not form thin discs, but rather extended puffed up ellipsoidal distributions similar to, for example, the stellar population of the isolated dwarf Wolf–Lundmark–Melotte (WLM). The scale length values we find are in reasonable agreement with other recent simulation of dwarf galaxies at this mass scale (e.g. Shen et al. 2014). In the case of SIDM1 and SIDM10, the presence of a small stellar core is visible in Fig. 5. The scale length does not change significantly as a function of the underlying DM model. However, it can clearly be seen that DM self-interactions lead to slightly larger exponential scale radii.

We note that, contrary to previous studies, we achieve exponential stellar surface density profiles without a bursty star formation model or a high-density threshold for star formation. We therefore find that our quiescent, smooth star formation model leads to non-exponential star formation histories, and to exponential stellar surface density profiles. It has been argued that these characteristics are intimately connected to 'bursty' star formation rates (see e.g. Governato et al. 2010). As a corollary, it was argued that the formation of a DM core is then naturally expected. However, we find that this is not necessarily the case. We should note that Teyssier et al. (2013) simulated an isolated dwarf of a similar halo mass and stellar mass as our dwarf dA but with a considerably bursty star formation model that produced an 800 pc core. This is in clear contrast to our simulation where baryonic effects are unable to create a DM core despite of the high global efficiency of star formation. The key is then, once more, in the time-scales and efficiency of energy injection during SNe-driven outflows. It remains to be seen if star formation histories in real dwarf galaxies occur in bursts with a time-scale much shorter than the local DM dynamical time-scale, and with an effective energy injection into the DM particles that is sufficient to significantly alter the DM distribution.

As we have shown above, halo dA is in relative isolation and has a quiet merger history. We therefore expect that the final stellar and DM configuration is nearly in equilibrium. In the case of SIDM, once the isothermal core forms, further collisions are not relevant anymore in changing the DM phase-space distribution. We can then ignore the collisional term in the Boltzmann equation and test the equilibrium hypothesis by solving the Jeans equation for the radial velocity dispersion profile using as input the density and anisotropy profiles:

$$\frac{1}{\rho}\frac{\mathrm{d}}{\mathrm{d}r}\left(\rho\sigma_r^2\right) + \frac{2\beta\sigma_r^2}{r} = -\frac{GM_{\mathrm{tot}}(<r)}{r^2}, \tag{7}$$

where $M_{\mathrm{tot}}(<r)$ is the total enclosed mass. We solve equation (7) independently for the collisionless components, DM and stars, using the fits to the density profiles with the analytic formulae introduced above. In addition, we also fit the corresponding radial anisotropy profiles for both the DM and the stars with the following five-parameter formula:

$$\beta(r) = A\left(\frac{r}{\mathrm{kpc}}\right)^a \mathrm{e}^{-\alpha\beta\left(\frac{r}{\mathrm{kpc}}\right)^b} + \beta_0. \tag{8}$$

The best-fitting parameters for this relation for each DM model are listed in Table 4.

The result obtained by solving the Jeans equation for the CDM and SIDM10 cases is seen in Fig. 6. Here we show the predicted dispersion profiles with dashed lines for DM (thick lines) and stars (thin lines). The solid lines show the actual simulation results. Although the agreement between the velocity dispersion predicted by the Jeans analysis and the simulation is not perfect, the comparison still indicates that halo dA is roughly in equilibrium and that the spherical approximations assumed above are partially correct. In the SIDM10 case, this would suggest that the dark matter core formed in the past and that any subsequent scattering does not affect the final equilibrium configuration once the galaxy forms. This would justify the use of the Jeans equation without considering a collisional term. We will consider a more detailed dynamical analysis in a subsequent paper analysing the different SIDM cases,

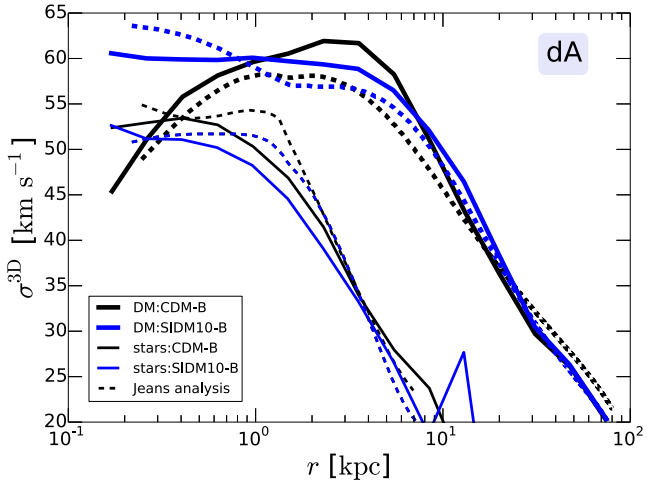

Figure 6. Velocity dispersion profiles for CDM (black) and SIDM10 (blue) compared to the results obtained with a Jeans analysis for halo dA. The DM profile is shown with thick lines, whereas the stellar profile is shown with thinner lines. Solid lines show the simulation results, whereas the results of the Jeans analysis are shown with dashed lines. The agreement between the Jeans analysis and the simulation suggests that the galactic system (DM halo+stars) is approximately in a collisionless spherical steady state. A similar analysis cannot be performed for halo dB since this halo is not relaxed due its merger history and environment, which is significantly more violent and less isolated than that of dA.

having a closer look at the velocity anisotropies and also investigating departures from spherical symmetry (Zavala & Vogelsberger, in preparation).

6 THE INNER HALO

In this section we study in more detail the matter content and structure of the simulated dwarf dA within the central region, ∼1 kpc, which roughly encloses the DM core size for all models.

We start with Fig. 7 which shows the mass build-up of DM (top) and stars (bottom) within 1 kpc as a function of time. In the cases with a constant scattering cross-section, it is clear that there is a significant amount of dark matter mass expelled from the central kiloparsec. In the case of SIDM1, for example, about 10^8 M$_\odot$ have been removed by $z = 0$. For the vdSIDM models, however, there is only a minimal deviation from the evolution of the base CDM model. In fact, the vdSIDMb model mass evolution follows the CDM result very closely and shows a nearly constant central mass after early times ∼1 Gyr. The vdSIDMa model leads to a small depletion of DM in the central 1 kpc of about $\sim 0.5 \times 10^8$ M$_\odot$. The largest depletion can be seen for the SIDM10 model, where the central mass is reduced by nearly a factor of 3.

The central stellar mass on the other hand grows steadily with time but it is at all times, and for all DM models, subdominant compared to the inner DM mass. For all models the central stellar mass is below 5×10^7 M$_\odot$ at $z = 0$, which is a factor of ∼5 lower than the central DM mass at that time. The stellar mass in SIDM1 and SIDM10 grows more slowly than in the CDM and vdSIDM cases. The vdSIDM models behave very similar to the CDM case, where the stellar mass grows nearly linearly with time reaching a mass of about 4×10^7 M$_\odot$. The stellar mass within 1 kpc grows initially similar SIDM10 (SIDM1), however, after ∼2 Gyr (∼4 Gyr) the stellar mass growth is slowed down for SIDM10 (SIDM1). After that time the growth is still linear but with a significantly shallower

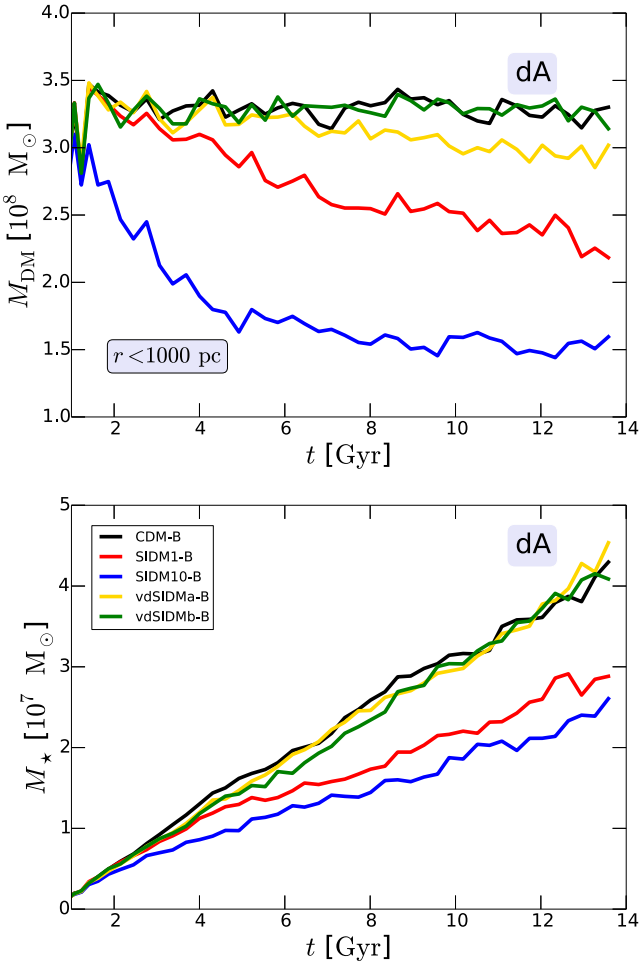

Figure 7. Time evolution of the enclosed masses measured within 1000 pc for DM (top) and stellar mass (bottom) for halo dA. The enclosed DM mass is for all times and for all models significantly larger than the stellar mass, and therefore dynamically dominates the centre of the dwarf. The central DM mass is substantially reduced for the SIDM1 and SIDM10 models, but only slightly for the vdSIDM models. Similarly, the stellar mass is only reduced for the models with constant cross-section, whereas the stellar mass growth of vdSIDM closely follows that of the CDM case.

slope compared to the CDM and vdSIDM cases. We note that SIDM1 is an allowed model, and it is striking how different its stellar mass is growing compared to the other allowed vdSIDM models.

To quantify this in more detail we present a closer look of the density profiles of DM (solid lines) and stars (dashed lines) in Fig. 8. This reveals a tight correlation between the shape of the DM and stellar density distributions. The stars within the core react to the change in the potential of the dominant DM component due to self-interactions. The size of the stellar core is therefore tied, to certain degree, to the core sizes of the DM distribution. In the cases where the scattering cross-section has a velocity dependence, although the creation of a DM core is evident, the impact is minimal in the stellar distribution compared to the models with a constant cross-section. This is mainly because even in the CDM case, the stellar distribution forms a core which is roughly the size of the DM core observed in the vdSIDM cases. We conclude that self-interactions drive the sizes of the cores in DM and stars to track each other. For SIDM1, the density within the core is a factor of ∼2–3 smaller than in CDM. The central distribution of stars can therefore probe the

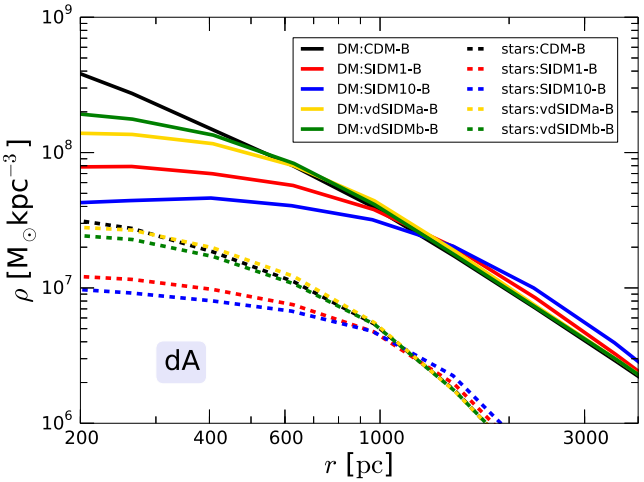

Figure 8. Density profile of halo dA for DM (solid) and stars (dashed) within the inner 4 kpc for the different DM models. The stars trace the evolution of DM and also form a core. The size of the stellar core is closely related to the size of the DM core. This can be seen most prominently for the SIDM1 and SIDM10 models.

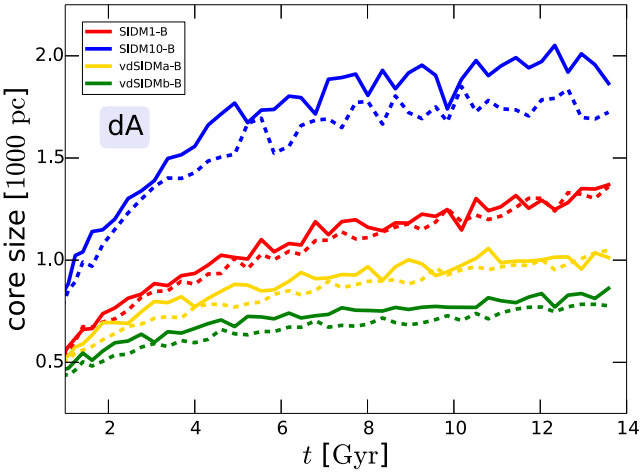

Figure 9. DM core size as a function of time for halo dA. We compare the evolution of the Burkert scale radius, r_b, in the DM-only simulations (dashed) with the simulations including baryons (solid). Baryons have only a tiny effect on the evolution and size of the cores. The largest effect can be seen for SIDM10, where the shallow DM profile allows SNe feedback to expand the core a bit more compared to the DM-only case.

nature of DM and can potentially be used to distinguish different SIDM models.

The strong correlation between DM and stars that we are finding is similar to the one suggested recently by Kaplinghat et al. (2014) using analytical arguments, but the regimes and interpretations are quite different. Whereas these authors investigated the response of SIDM to a dominant stellar component, we are investigating a system where DM still dominates dynamically. Thus in the former, the DM cores sizes are reduced relative to expectations from DM-only simulations due to the formation of the galaxy, while in the latter, the stellar distribution of the galaxy responds to the formation of the SIDM core by increasing its own stellar core relative to the CDM case. This regime is therefore more promising to derive constraints for the nature of DM.

Next we are interested in the time evolution of the core radii. It was already obvious from Fig. 7 that for the largest cross-section cases, the core should already be present early on during the formation history of the galaxy. This is indeed the case as we demonstrate more clearly in Fig. 9, where the evolution of the core sizes is shown as a function of time. As a measure of core radius, we fit Burkert profiles (Burkert 1995) at each time, for each of the models, to extract the core size r_B:

$$\rho_B(r) = \rho_B \frac{r_B^3}{(r + r_B)(r^2 + r_B^2)}. \quad (9)$$

We note that we use this two-parameter fit for simplicity to fit all SIDM models and give a measure of the core size. As we explored in detail above, the different SIDM models are actually better fitted by different radial profiles. However, our purpose here is not to rigorously define a core size but simply to present an evolutionary trend for the different models. This trend is clearly visible in the figure as well as the dependence of the amplitude of the core size on the scattering cross-section. Fig. 9 shows the core radii determined by these two-parametric Burkert fits for all DM models with (solid lines) and without (dashed lines) the effects baryons.

Fig. 9 also demonstrates that the actual impact of baryons on the DM distribution relative to the DM-only case is minor, as we discussed already above (see lower right-hand panel of Fig. 4). In the case of CDM this is not surprising since: (i) our star formation model is less bursty compared to models where the cusp-core transformation is efficient and (ii) for the mass scale we are considering, halo mass $\sim 10^{10}$ M$_\odot$ for halo dA, the energy released by SNe is not expected to be sufficient to create sizeable DM cores (Governato et al. 2012; Peñarrubia et al. 2012; Garrison-Kimmel et al. 2013), although see Teyssier et al. (2013). Fig. 9 demonstrates that our star formation and feedback model creates only a slightly larger core for the SIDM10 model. This is because expelling gas in this case is easier due to the reduced potential well caused by DM collisions. We stress again that these results are sensitive to the model used for SNe-driven energy injection into the DM particles (both efficiency and time-scales). Larger efficiencies of energy injection into shorter time-scales would result in a larger removal of DM mass from the inner halo.

According to Fig. 9 a sizeable core is already present very early on. By $t = 4$ Gyr all the models already have cores more than half of their present-day size. Furthermore, Fig. 9 also demonstrates that none of our SIDM models leads to the gravothermal catastrophe where the core collapses following the outward flux of energy caused by collisions. This is consistent with the findings in VZL, where only one subhalo, with similar total dark matter mass as halo dA, of the analogous SIDM10 MW-size simulation was found to enter that regime towards $z = 0$.

As a consequence of the DM core settling early on in the formation history of the galaxy, the star formation rate within the central 1 kpc is reduced significantly at late times in the cases with constant cross-section. This results in a stellar population that is in average older than in the case of CDM. This is clearly shown in Fig. 10, where we plot the time evolution of the ratio of the metallicity averaged within the central 1 kpc, relative to the CDM case. The difference today is $\gtrsim$10 per cent. Interestingly, in the vdSIDM cases, there is an excess in star formation within 1 kpc in the last stages of the evolution resulting in a younger stellar population since the last $\sim$2 Gyr (see also Fig. 9). We will investigate this issue, and in general the properties of the central $\sim$ kpc region, in a follow-up paper using simulations with increased resolution (Zavala & Vogelsberger, in preparation).

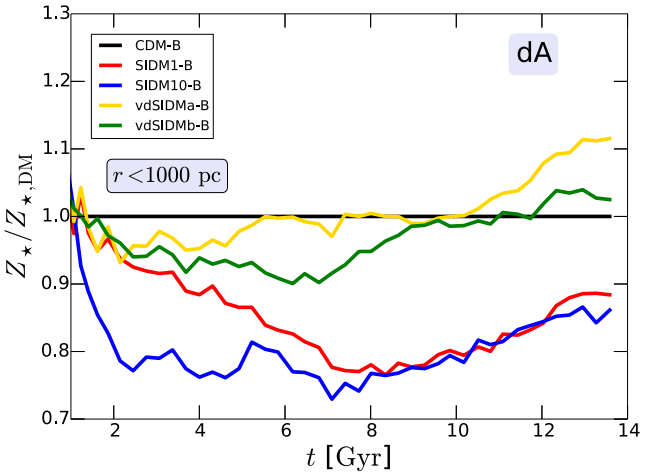

Figure 10. Evolution of the central stellar metallicity (within 1 kpc). We show the ratios of the different models with respect to the CDM case. The cases with a constant cross-section lead to a significant suppression of the central stellar metallicity at $z = 0$. The vdSIDM models have a weaker impact.

In Fig. 11 we focus on a region even closer to the halo centre and show the total mass within 500 pc (top) and the slope of the density profile measured at this radius (bottom). We compare both to observational estimates using samples of dwarf galaxies compiled in Kuzio de Naray & McGaugh (2014; top) and from the H I Nearby Galaxy Survey (THINGS; bottom; Walter et al. 2008). At these small radii, the change in the enclosed mass is still more dramatic for the constant cross-section SIDM models having a deficit in mass by a factor of $\gtrsim 3$ relative to the CDM case, while the vdSIDM cases, although close to CDM, still deviate visibly. The logarithmic slope of the density profile at this radius varies between -0.3 (SIDM10) and -1.3 (CDM). Fig. 11 shows that given the large dispersion in the data, all DM models are essentially consistent with observations. There is however some tension with the CDM simulation of halo dA having a slightly too large total mass, and a slightly too steep DM density slope at $r = 500$ pc. On the other hand, the SIDM10 case might be too cored for the stellar mass of halo dB ($M_\star \sim 10^9\,\mathrm{M}_\odot$). Taking both haloes into account, and looking at the two relations of Fig. 11 only, it seems that SIDM1 agrees best with these observations. We stress, however, that our dwarf sample is far to small to draw any conclusions based on this result and these observations are in any case, too uncertain to use them as constraints.

7 CONCLUSION

SIDM is one the most viable alternatives to the prevailing CDM paradigm. Current limits on the elastic scattering cross-section between DM particles are set at $\sigma/m_\chi < 1\,\mathrm{cm}^2\,\mathrm{g}^{-1}$ (Peter et al. 2013). At this level, the DM phase-space distribution is altered significantly relative to CDM in the centre of DM haloes. The impact of DM self-interactions on the baryonic component of galaxies that form and evolve in SIDM haloes has not been explored so far. Recently, Kaplinghat et al. (2014) analytically estimated the DM equilibrium configuration that results from a stellar distribution added to the centre of a halo in the case of SIDM. These authors studied the regime where the stellar component dominates the gravitational potential and concluded that the DM core sizes (densities) are smaller (higher) than observed in DM-only SIDM simulations.

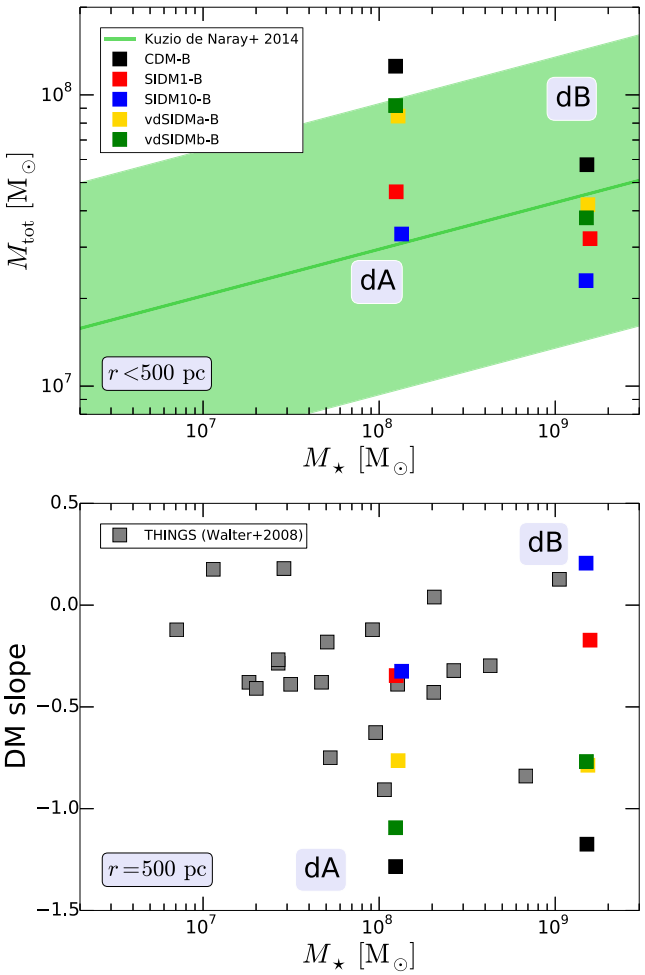

Figure 11. Top panel: enclosed total mass within 500 pc as a function of total stellar mass. Bottom panel: DM density slope at 500 pc as a function of total stellar mass. The different DM models lead to significantly different slopes and masses at and within 500 pc. At this radius even the vdSIDM models clearly deviate from the CDM case. Both the mass and the slope clearly scale with the cross-section and allow to disentangle the different DM models. Observational estimates from a combined sample of dwarf galaxies (Kuzio de Naray & McGaugh 2014) and from the THINGS survey (Walter et al. 2008) are also shown in the top and bottom panels, respectively.

This might have important consequences on current constraints of SIDM models since they have been derived precisely in the baryon-dominated regime. In this paper we explore the opposite regime that of dwarf galaxies where DM dominates the gravitational potential even in the innermost regions. Our analysis is based on the first hydrodynamical simulations performed in a SIDM cosmology. We focus most of the analysis on a single dwarf with a halo mass $\sim 1.1 \times 10^{10}\,\mathrm{M}_\odot$. We study two cases with a constant cross-section: SIDM1 and SIDM10, $\sigma/m_\chi = 1$ and $10\,\mathrm{cm}^2\,\mathrm{g}^{-1}$, respectively, and two cases with a velocity-dependent cross-section: vdSIDMa–b, that were also studied in detail in VZL and Zavala et al. (2013). Except for SIDM10, all these models are consistent with astrophysical constraints, solve the 'too big to fail' problem and create $\mathcal{O}(1\,\mathrm{kpc})$ cores in dwarf-scale haloes.

Our simulations include baryonic physics using the implementation described in Vogelsberger et al. (2013) employing the moving mesh code AREPO (Springel 2010). We use the same model that was set up to reproduce the properties of galaxies at slightly larger

mass-scales. Our intention in this first analysis is not to match the properties of dwarf galaxies precisely, but rather to compare SIDM and CDM with a single prescription for the baryonic physics, which has been thoroughly tested on larger scales.

Our most important findings are the following:

Impact of SIDM on global baryonic properties of dwarf galaxies. The stellar and gas content of our simulated dwarfs agree reasonably well with various observations including the stellar mass as a function of halo mass, the luminosity–metallicity relation, the neutral hydrogen content and the cumulative star formation histories. The latter are similar to those of local isolated group dwarf galaxies with similar stellar masses. We find that the stellar mass, the gas content, the stellar metallicities and star formation rates are only minimally affected by DM collisions in allowed SIDM models. The allowed elastic cross-sections are too small to have a significant global impact on these quantities, and the relative differences between the different DM models are typically less than $\sim$10 per cent. In most cases these changes are not systematic as a function of the employed DM model. The modifications in the global baryonic component of the galaxies can therefore not be used to constrain SIDM models since the effects are too small and not systematic.

Impact of SIDM on the inner halo region. Within $\sim$1 kpc, we find substantial differences driven by the collisional nature of SIDM. Besides the well-known effect of SIDM on the DM density profiles, we also find that at these scales the distribution of baryons is significantly affected by DM self-interactions. Both stars and gas show relative differences up to $\sim$50 per cent in the density, the velocity dispersion and the gas temperature. Most of the effects increase with the size of the cross-section in the central region. The strongest correlation with the cross-section can be found for the stellar profiles, where the central stellar density profile clearly correlates with the central cross-section leading to lower central densities for DM models with larger central cross-sections.

Impact of baryons on the inner halo region. We find that the impact of baryons on the DM density profile is small for the DM-dominated dwarf ($M_\star/M_{\rm DM}(<1\,{\rm kpc}) \lesssim 0.15$) studied here. However, this result is also connected to our smooth star formation model, which is not as bursty as models where a significant core formation is observed due to baryonic feedback. The size of the DM core and the central density are therefore essentially the same as in our simulations that have no baryons, although the core size is slightly larger in the former than in the latter.

Disentangling different SIDM models. For the cases where the scattering cross-section is constant, the combination of two key processes: (i) an early DM core formation such that by $t = 4$ Gyr, the DM cores already have half of their size today; and (ii) a star formation history dominated by the period after the formation of the DM core, result in the following characteristics of the stellar distribution of SIDM galaxies. (a) The development of a central stellar core with a size that correlates with the amplitude of the scattering cross-section. For instance, for the SIDM1 case with $\sigma/m_\chi = 1\,{\rm cm^2\,g^{-1}}$, the density within the stellar core is a factor of $\sim$2–3 smaller than for the CDM case. (b) A reduced stellar mass in the sub-kpc region ($\gtrsim$30 per cent) as a by-product of the reduced DM gravitational potential due to self-scattering. (c) A reduced central stellar metallicity; by $\gtrsim$10 per cent at $z = 0$ compared to the CDM case. Around $z \sim 1$ the metallicity can be reduced by up to $\sim$25 per cent.

For the cases where the scattering cross-section is velocity dependent, even though a sizeable DM core can still be created ($\sim$400 pc), the effect in the stellar distribution at all scales is minimal relative to CDM. This is likely because the amplitude of the cross-section within the inner region of the dwarf is not large enough to produce a DM core that is larger than the stellar core that forms in the CDM case. Whether the latter could be the result of numerical resolution is something we will investigate in a forthcoming paper. Any changes that we found in the vdSIDM cases seem to be only related to the stochastic nature of the simulated star formation and galactic wind processes.

These conclusions are key predictions of SIDM that can in principle be tested to either constrain currently allowed models, particularly constant cross-section models, or to find signatures of DM collisions in the properties of the central stellar distributions of dwarf galaxies. In future works we will explore these possibilities in more detail.

ACKNOWLEDGEMENTS

We thank Daniel Weisz for providing cumulative star formation histories of Local Group dwarfs to us, and Michael Boylan-Kolchin for help with the initial conditions. We further thank Volker Springel for useful comments and giving us access to the AREPO code. The Dark Cosmology Centre is funded by the DNRF. JZ is supported by the EU under a Marie Curie International Incoming Fellowship, contract PIIF-GA-2013-627723. The initial conditions were made using the DiRAC Data Centric System at Durham University, operated by the Institute for Computational Cosmology on behalf of the STFC DiRAC HPC Facility (www.dirac.ac.uk). The DiRAC system is funded by BIS National E-infrastructure capital grant ST/K00042X/1, STFC capital grant ST/H008519/1, STFC DiRAC Operations grant ST/K003267/1 and Durham University. DiRAC is part of the Re: green card UK National E-infrastructure.

REFERENCES

Amorisco N. C., Zavala J., de Boer T. J. L., 2014, ApJ, 782, L39
Arkani-Hamed N., Finkbeiner D. P., Slatyer T. R., Weiner N., 2009, Phys. Rev. D, 79, 015014
Arraki K. S., Klypin A., More S., Trujillo-Gomez S., 2014, MNRAS, 438, 1466
Behroozi P. S., Wechsler R. H., Conroy C., 2013, ApJ, 770, 57
Boehm C., Schewtschenko J. A., Wilkinson R. J., Baugh C. M., Pascoli S., 2014, preprint (arXiv:1404.7012)
Boylan-Kolchin M., Springel V., White S. D. M., Jenkins A., Lemson G., 2009, MNRAS, 398, 1150
Boylan-Kolchin M., Bullock J. S., Kaplinghat M., 2011, MNRAS, 415, L40
Boylan-Kolchin M., Bullock J. S., Kaplinghat M., 2012, MNRAS, 422, 1203
Breddels M. A., Helmi A., 2013, A&A, 558, A35
Brooks A. M., Kuhlen M., Zolotov A., Hooper D., 2013, ApJ, 765, 22
Buckley M. R., Zavala J., Cyr-Racine F.-Y., Sigurdson K., Vogelsberger M., 2014, preprint (arXiv:1405.2075)
Burkert A., 1995, ApJ, 447, L25
Cline J. M., Liu Z., Moore G. D., Xue W., 2014, Phys. Rev. D, 89, 043514
Côté S., Carignan C., Freeman K. C., 2000, AJ, 120, 3027
Cyr-Racine F.-Y., Sigurdson K., 2013, Phys. Rev. D, 87, 103515
de Blok W. J. G., Walter F., Brinks E., Trachternach C., Oh S.-H., Kennicutt R. C., Jr, 2008, AJ, 136, 2648
Feng J. L., Kaplinghat M., Tu H., Yu H.-B., 2009, J. Cosmol. Astropart. Phys., 7, 4
Feng J. L., Kaplinghat M., Yu H.-B., 2010, Phys. Rev. Lett., 104, 151301
Ferrero I., Abadi M. G., Navarro J. F., Sales L. V., Gurovich S., 2012, MNRAS, 425, 2817
Garrison-Kimmel S., Rocha M., Boylan-Kolchin M., Bullock J. S., Lally J., 2013, MNRAS, 433, 3539
Genel S. et al., 2014, preprint (arXiv:1405.3749)

Governato F. et al., 2010, Nature, 463, 203
Governato F. et al., 2012, MNRAS, 422, 1231
Hopkins P. F., Keres D., Onorbe J., Faucher-Giguere C.-A., Quataert E., Murray N., Bullock J. S., 2013, preprint (arXiv:1311.2073)
Huang S., Haynes M. P., Giovanelli R., Brinchmann J., Stierwalt S., Neff S. G., 2012, AJ, 143, 133
Kaplinghat M., Keeley R. E., Linden T., Yu H.-B., 2014, Phys. Rev. Lett., 113, 021302
Kauffmann G., 2014, preprint (arXiv:1401.8091)
Kirby E. N., Cohen J. G., Guhathakurta P., Cheng L., Bullock J. S., Gallazzi A., 2013, ApJ, 779, 102
Kirby E. N., Bullock J. S., Boylan-Kolchin M., Kaplinghat M., Cohen J. G., 2014, MNRAS, 439, 1015
Kuzio de Naray R., McGaugh S. S., 2014, ApJ, 782, L12
Kuzio de Naray R., McGaugh S. S., de Blok W. J. G., 2008, ApJ, 676, 920
Leaman R. et al., 2012, ApJ, 750, 33
Loeb A., Weiner N., 2011, Phys. Rev. Lett., 106, 171302
McGaugh S. S., 2005, ApJ, 632, 859
Marinacci F., Pakmor R., Springel V., 2014a, MNRAS, 437, 1750
Marinacci F., Pakmor R., Springel V., Simpson C. M., 2014b, MNRAS, 442, 3745
Misgeld I., Hilker M., 2011, MNRAS, 414, 3699
Moster B. P., Naab T., White S. D. M., 2013, MNRAS, 428, 3121
Navarro J. F., Eke V. R., Frenk C. S., 1996, MNRAS, 283, L72
Oh S.-H., de Blok W. J. G., Walter F., Brinks E., Kennicutt R. C., Jr, 2008, AJ, 136, 2761
Oh S.-H., de Blok W. J. G., Brinks E., Walter F., Kennicutt R. C., Jr, 2011, AJ, 141, 193
Pakmor R., Marinacci F., Springel V., 2014, ApJ, 783, L20
Peñarrubia J., McConnachie A. W., Navarro J. F., 2008, ApJ, 672, 904
Peñarrubia J., Pontzen A., Walker M. G., Koposov S. E., 2012, ApJ, 759, L42
Peter A. H. G., Rocha M., Bullock J. S., Kaplinghat M., 2013, MNRAS, 430, 105
Pontzen A., Governato F., 2012, MNRAS, 421, 3464
Rocha M., Peter A. H. G., Bullock J. S., Kaplinghat M., Garrison-Kimmel S., Oñorbe J., Moustakas L. A., 2013, MNRAS, 430, 81
Sawala T. et al., 2014, preprint (arXiv:1404.3724)
Shen S., Madau P., Conroy C., Governato F., Mayer L., 2014, ApJ, 792, 99
Spergel D. N., Steinhardt P. J., 2000, Phys. Rev. Lett., 84, 3760
Springel V., 2010, MNRAS, 401, 791
Springel V. et al., 2008, MNRAS, 391, 1685
Stark D. V., McGaugh S. S., Swaters R. A., 2009, AJ, 138, 392
Teyssier R., Pontzen A., Dubois Y., Read J. I., 2013, MNRAS, 429, 3068
Tollerud E. J. et al., 2012, ApJ, 752, 45
Torrey P., Vogelsberger M., Genel S., Sijacki D., Springel V., Hernquist L., 2014, MNRAS, 438, 1985
Tulin S., Yu H.-B., Zurek K. M., 2013, Phys. Rev. D, 87, 115007
van den Aarssen L. G., Bringmann T., Pfrommer C., 2012, Phys. Rev. Lett., 109, 231301
Vogelsberger M., Zavala J., 2013, MNRAS, 430, 1722
Vogelsberger M., Zavala J., Loeb A., 2012, MNRAS, 423, 3740 (VZL)
Vogelsberger M., Genel S., Sijacki D., Torrey P., Springel V., Hernquist L., 2013, MNRAS, 436, 3031
Vogelsberger M. et al., 2014a, Nature, 509, 177
Vogelsberger M. et al., 2014b, preprint (arXiv:1405.2921)
Walker M. G., Peñarrubia J., 2011, ApJ, 742, 20
Walter F., Brinks E., de Blok W. J. G., Bigiel F., Kennicutt R. C., Jr, Thornley M. D., Leroy A., 2008, AJ, 136, 2563
Weisz D. R., Dolphin A. E., Skillman E. D., Holtzman J., Gilbert K. M., Dalcanton J. J., Williams B. F., 2014, ApJ, 789, 147
Woo J., Courteau S., Dekel A., 2008, MNRAS, 390, 1453
Zavala J., Vogelsberger M., Walker M. G., 2013, MNRAS, 431, L20
Zolotov A. et al., 2012, ApJ, 761, 71

This paper has been typeset from a TEX/LATEX file prepared by the author.